Journal of Applied Polymer Science

Quaternized poly(phenylene oxide) anion exchange membrane for alkaline direct methanol fuel cells in KOH-free media

K. Hari Gopi,[1] Santoshkumar D. Bhat,[1] Akhila Kumar Sahu,[1] P. Sridhar[2]

[1]CSIR-Central Electrochemical Research Institute-Madras Unit, Taramani, Chennai 600113, Tamilnadu, India

[2]Mesha Energy Solutions Pvt. Ltd., Yeshwantpur, Bangalore, Karnataka, India

Correspondence to: S. D. Bhat (E-mail: sdbhat@cecri.res.in)

ABSTRACT: A series of anion exchange membrane (AEM) electrolytes with quaternary ammonium moiety are fabricated from poly (phenylene oxide) for its application in alkaline direct methanol fuel cells (ADMFCs). In the first step, poly(phenylene oxide) (PPO) is successfully chloromethylated by substituting chloromethyl groups in the aryl position of polymer. In the second step, the chloromethylated PPO (CPPO) is further homogeneously quaternized and ion-exchanged to form an AEM. From the second step, series of AEMs are prepared by changing the mole ratio of amine in relation to CPPO. The presence of quaternary ammonium group in the membrane was confirmed by elemental analysis. The fabricated membranes are subjected to cell polarization studies in ADMFCs, wherein quaternized poly(2,6-dimethyl-1,4-phenylene oxide) (CPPO:amine of 1:8) membrane exhibits higher peak power density of 3.5 mW cm^{-2} when compared with the other ratios of CPPO:amine in the absence of KOH solution. © 2016 Wiley Periodicals, Inc. J. Appl. Polym. Sci. **2016**, *133*, 43693.

KEYWORDS: electrochemistry; fuel cells; functionalization of polymers; membranes; polyelectrolytes

Received 28 December 2015; accepted 26 March 2016

DOI: 10.1002/app.43693

INTRODUCTION

Direct methanol fuel cells (DMFCs) are applied widely in portable and other stationary applications considering its potential as a power source due to its high energy density, ease of storage, and use of liquid as a fuel without any humidification.[1,2] Many researchers have reported high power density for DMFCs using proton exchange membranes (PEMs).[3,4] However DMFC based on PEMs suffer from many limitations such as slow reaction kinetics at anode, methanol cross-over through the membrane, and high utilization of Pt-based catalyst in conjunction to cost related issues.[5] By shifting the medium from acidic to alkaline, the above said drawbacks can be addressed.

Recently, there has been renewed interest in alkaline membrane direct methanol fuel cells (ADMFCs) which replace the PEM with anion exchange membrane (AEM).[6] When the working environment is alkaline, methanol oxidation kinetics will be faster than acidic media, thus allowing the use of abundant low cost non-noble metal electrocatalysts like Ni, Fe, and Ag.[7] Moreover, the issue of methanol crossover will be curtailed by the electro-osmotic movement of ions transported from cathode to anode, thus opposing the flow of methanol. Since the ion transport will be from the cathode to anode, water is now produced at the anode and consumed at the cathode. Thus the water management regime is altered and potentially simplified; also the problem of flooding at the cathode is avoided.[8]

AEM is the key component for ADMFCs as anion conductor. AEMs are the positively charged electrolyte acting as the charge carrier [usually quaternary ammonium (QA) type] grafted on the polymer backbone with dissociated anions for ionic conductance.[9] Polymer electroneutrality is maintained by attaching a mobile counter-ion to each ionic functional group. The choice of AEM to be used as solid electrolyte demands high OH^- conductivity with excellent methanol tolerance and good chemical stability. Several different cationic head-group chemistry are available in the literature based on QA,[10] phosphonium,[11] guanidinium,[12] and imidazolium type[13] which not only acts as charge carrier for OH^- ion transport but also improves the chemical stability of membranes.[9] Till date, the QA has been the most extensively studied anion conductive head group in AEMs due to the ease of preparation and low cost.[14]

Typically, AEMs are synthesized by two reaction steps. In the first step, reactive chloromethyl groups are attached to the polymer backbone by chloromethylation reaction. In the second step, quaternization with tertiary amine such as trimethylamine

Table I. Effect of Reaction Time on the Chloromethylation Reaction

CMEE:PPO (mol:mol)	Reaction time (h)	Substitution degree[a] (%)	Membrane property	Water uptake (at 30 °C)
1:0.5	5	40	Stable	35
1:0.5	6	49	Stable	45
1:0.5	8	57	Stable	57
1:0.5	10	62	Swelling	69
1:0.5	20	66	Swelling	82

[a] Calculated from ^{1}H NMR spectra.[28]

was done to form a QA moiety. There are several reports on AEM developed from variety of polymers like polysulfone,[15] poly(arylene ether sulfone),[16] poly(ether ether ketone),[17] poly (arylene ether),[18] poly(phenylene oxide),[19] poly(epichlorohydrin),[20] and polybenzimidazole.[21] Yang *et al.* reported the preparation of AEMs by incorporating inorganic fillers such as silica, alumina, and titania to form a composite membrane for its evaluation in ADMFCs.[22] Wan *et al.*[23] prepared a series of quaternized-chitosan derivatives with various degree of quaternization (DQ) using glycidyltrimethyl ammonium chloride as quaternization agent. Zhang *et al.*[24] prepared a series of fluoropolymer AEMs by copolymerization of vinylbenzyl chloride (VBC) with fluoroalkylacrylate & butyl methacrylate and evaluated their APEFC performance.

PPO is one of the widely used thermoplastic for the preparation of ion exchange membranes because of its easy accessibility, good solubility, high chemical and thermal stability.[25] Generally, PPO is used as a precursor for the preparation of various functional polymers by chemical modification either in their aryl or benzylic positions for its use as solid polymer electrolyte. Janarthanan *et al.*[25] investigated the performance of poly(phenylene)-based AEM in a DMFC with different anode gas diffusion layers using two commercially available platinum catalysts supported on carbon. Katzfuß et al.[26] developed an AEM from 1,5-dimethylpolyphenylenoxide by using N-bromosuccinimide as brominating reagent. The brominated PPO was further cross-linked with DABCO to form a covalent cross-linked membrane used for ADMFCs.

In view of the above, the present study focuses on developing series of AEMs from poly(phenylene oxide) via chloromethylation followed by Menshutkin reaction methodology[27] for quaternization and its application as a solid electrolyte for ADMFC in a KOH free fuel. In the present study, initially the influence of reaction time on the chloromethylation reaction was investigated. In the second process, an *in situ* method for quaternization was followed and the impact of amination by varying the amount of amine to polymer ratio was studied in detail. A series of membranes with different DQ are prepared and evaluated for its ionic conductivity, ion exchange capacity (IEC), and single-cell DMFC performance. During cell polarization measurements, the influence of metal loading in the catalyst layer and the durability of membrane at open circuit voltage (OCV) were also investigated. The chemical stability of the optimized membrane at high pH and temperature was also investigated for several hours.

EXPERIMENTAL

Synthesis of Chloromethylated Poly(2,6-dimethyl-1,4-phenylene oxide) (CPPO)

The chloromethylation of poly(2,6-dimethyl-l,4-phenylene oxide) (Sigma–Aldrich, India) was carried out as reported in our earlier literature[28,29] In brief, in a 100 mL dried three-neck round bottom flask, 1.5 g of PPO was dissolved in 15 mL of chlorobenzene (Merck, India) at 30 °C, followed by addition of zinc chloride catalyst (0.075 g) (Acros Organics, India). Chloromethyl ethyl ether (CMEE, 2.3 mL, 0.025 mol) (Acros Organics, India) was added drop-wise to the reaction flask containing PPO solution. The reaction mixture was stirred at 50 °C for different time intervals as mentioned in Table I. At the end of each time interval, the reaction mixture was cooled to room temperature and precipitated using methanol to form CPPO which was filtered and washed with distilled water. The product was dried in a vacuum oven at 60 °C to form a spongy white powder (1.9 g, 90% yield). The degree of substitution (DS) was calculated from the ^{1}H NMR spectra for different time intervals accordingly.[28]

Synthesis of Quaternized Poly(2,6-dimethyl-1,4-phenylene oxide) (QPPO)

The quaternization of CPPO was done by an *in situ* homogenous amination.[29] The dried CPPO precipitate (0.6 g) was dissolved in N-Methyl-2-pyrrolidone (Acros Organics, India) at 50 °C to prepare 3 wt % solution. After cooling to room temperature, trimethylamine solution (30 wt % in water) in different mole ratios (as represented in Table II) with respect to CPPO was added. The reaction mixture was stirred for 24 h at 30 °C to introduce QA groups using trimethylamine, which provide sufficient stability to polymer after casting. The solution was cast uniformly on a flat glass plate, and dried at 75 °C in a vacuum oven to form series of quaternized membranes namely QPPO 1 (with 1:4), QPPO 2 (with 1:6), QPPO 3 (with 1:8),

Table II. Effect of Amination on the Properties of Membrane

Membranes	CPPO: amine (mol:mol)	DQ (%)	IEC (mmol g^{-1})	Ionic conductivity at 30 °C (mS cm^{-1})
QPPO 1	1:4	4.20	0.83	5.5
QPPO 2	1:6	4.25	1.13	6.5
QPPO 3	1:8	4.31	1.38	7.6
QPPO 4	1:10	4.22	0.95	5.9

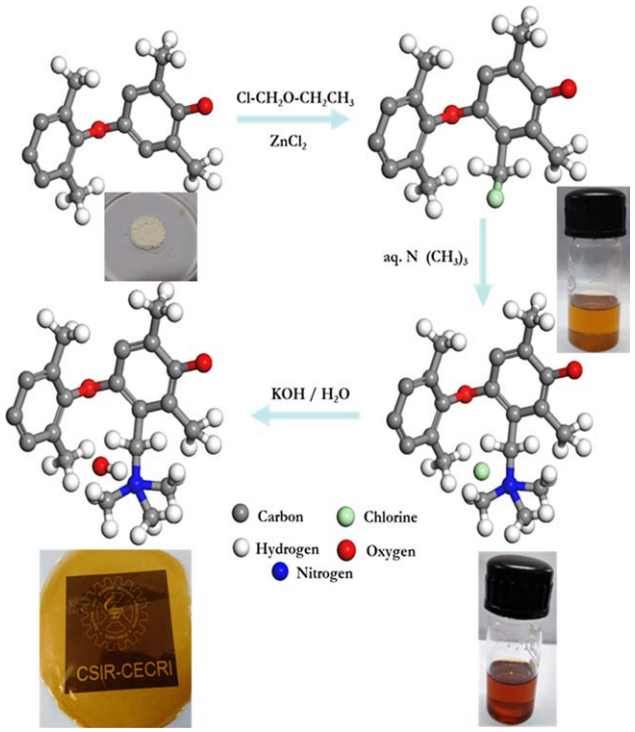

Figure 1. Ball & Stick model representing the preparation of QPPO. [Color figure can be viewed in the online issue, which is available at wileyonlinelibrary.com.]

and QPPO 4 (with 1:10) ratio. The dried Cl^- form of QPPO membranes were ion-exchanged to OH^- form by immersing in 2 mol dm^{-3} KOH solution at room temperature for 24 h. Finally, the membranes were repeatedly washed with deionized water to remove residual KOH and stored in deionized water prior to use. The thickness of the QPPO membranes was in the range of 130–150 μm. The Ball-Stick model of the whole reaction is presented as a scheme in Figure 1 along with step-to-step photographs of the product.

Physicochemical Characterization

Proton (^{1}H) NMR spectroscopy was used to confirm the synthesis of CPPO and also to determine the DS. ^{1}H NMR spectra were recorded on Bruker AVANCE spectrometer at a resonance frequency of 400 MHz using chloroform-d_1 ($CDCl_3$) as solvent and tetramethylsilane as an internal reference. A TG-DSC analyzer (NETZSCH, Model STA-449F3) was used to investigate the thermal stability of QPPO membranes. Samples of about 5–10 mg are loaded in to the alumina pan and heated over a temperature range of 30–800 °C. The measurements were carried out under nitrogen atmosphere at a heating rate of 5 °C min^{-1}. Topological and phase images of PPO and QPPO membranes were captured by tapping mode atomic force microscopy (PicoSPM-Picoscan 2100, Molecular Imaging). The nitrogen content in the QPPO membranes measured by Elementar Vario elemental analysis (Model EL III, Germany) was used, to determine the DQ from the following equation:

$$\mathrm{DQ}\,(\%) = \frac{\mathrm{X}/14}{[(100 - 227.5X)/120] + \mathrm{X}/14} \times 100, \qquad (1)$$

where X is the content of nitrogen obtained from CHNS analysis, 227.5 and 120 are the molecular weights of QPPO and PPO repeat units, respectively, and 14 is the atomic weight of nitrogen.

Water Sorption and IEC

Water sorption is an important characteristic property of a membrane which influences the ionic conductivity.[30] The water sorption was determined by measuring the difference in weight of membrane before immersion (dry membrane) and after immersion (wet membrane). At first, the quaternized membranes in Cl^- form were dried at 70 °C under vacuum for 24 h until a constant weight (W_d) was attained. The dry membranes were immersed in sorption chamber containing deionized water and equilibrated for at least 24 h at 30 °C. Then the membrane was taken out, surface sorbed and the weight of wet membrane (W_w) was measured immediately. The measurements were done in triplicate and the results obtained are within the standard deviation of ±0.2. The percentage of water sorption (W_s) was calculated from the following equation:

$$W_s(\%) = \frac{W_w - W_d}{W_d} \times 100, \qquad (2)$$

where W_w is the weight of wet membranes immersed in deionized water and W_d is the weight of dry membranes, respectively.

IEC was calculated using the Mohr's titration method as reported in our earlier study.[28] A weighed membrane sample (in its Cl^- form) was immersed in 0.5 mol dm^{-3} Na_2SO_4 for 8 h to convert the membrane from chloride (Cl^-) to sulfate ($SO4^{2-}$) form. The released chloride ions from the membrane were back-titrated using 0.1 mol dm^{-3} $AgNO_3$ solution with potassium chromate (0.25 mol dm^{-3}) as indicator. Similarly, blank titration was also performed without the membrane. By quantifying the amount of $AgNO_3$ consumed, the amount of chloride ions exchanged can be determined.

The IEC was determined from the following equation:

$$\mathrm{IEC}\left(\mathrm{mmol\ g^{-1}}\right) = \frac{\mathrm{Volume\ of\ AgNO_3} \times \mathrm{molarity\ of\ AgNO_3}}{\mathrm{Dry\ sample\ weight}}. \qquad (3)$$

Ionic Conductivity

The chloride ion (Cl^-) conductivity of the membranes were measured by two-probe AC impedance technique using Autolab PGSTAT 30 (Eco Chemie, Netherlands with FRA2 module) under potentiostatic mode over the frequency range of 1 MHz–1 Hz as described in our earlier literature.[28] In brief, prior to the conductivity measurements, the membrane samples were equilibrated by immersing in deionized water for 24 h. The in-house conductivity cell comprising two stainless-steel electrodes, each with 20 mm diameter was used for this study. The membrane samples were sandwiched between the two electrodes, fixed to a Teflon block and placed in a sealed glass chamber containing deionized water (100% relative humidity). The spectra were viewed as imaginary component of Z'' on the y-axis and the real component of Z' on the x axis. The resistance (R) of each membrane were determined from the Nyquist impedance plot through the intersection of high-frequency intercept with real axis, and thus conductivity is calculated. The

conductivity was recorded at different temperatures ranging from 30 to 70 °C.

The ionic conductivity (σ) for a particular membrane can be calculated using:

$$\sigma = \frac{L}{R \times A}, \quad (4)$$

where L is the thickness of membrane (cm), A is the cross-sectional area (cm^2), and R is the membrane resistance (Ω).

Methanol Permeability Studies

Methanol permeability of the membranes was measured using a single cell, under OCV conditions as described in our literature.[31] In brief, 2 mol dm^{-3} methanol was initially supplied to the cell and was allowed to equilibrate for 30 min. After attaining steady state, the difference in the amount of methanol supplied to the cell and the amount of methanol collected at the anode outlet, for a particular time (t), was measured at OCV under ambient pressure. The concentration of methanol diffused through the membrane was determined by sampling a small amount (1.0 μL) of the solution from the inlet and outlet of the cell by gas chromatography (Thermo Fisher Scientific, Trace GC 700 with capillary column and FID detector). It is to be noted that under OCV condition, methanol supplied at the inlet ($MeOH_{in}$) is equal to sum of methanol collected at the outlet ($MeOH_{out}$) and methanol permeated ($MeOH_{permeated}$) from anode to cathode, which is determined by the following relation:

$$MeOH_{permeability} = \frac{\Delta V \times \Delta C}{t \times A}, \quad (5)$$

where $MeOH_{permeability}$ is the permeability of membrane, ΔV is the difference in volume between the inlet and outlet solution, ΔC is the concentration difference between the inlet and outlet solution, t is the time after 5 h, and A is the effective area of membrane electrode assembly (MEA).

Alkaline Stability

Mostly, the alkaline resistance of AEMs are examined by their change in ionic conductivity before and after immersion in highly concentrated alkaline solution at higher temperature.[32] The optimized membrane (QPPO 3) in its chloride form was immersed in 4 mol dm^{-3} KOH solution at 75 °C to assess its alkaline stability. The membrane was kept immersed in a sealed vessel containing alkaline solution for 300 h by constantly replacing the solution for every 50 h. Then the sample was taken out washed thoroughly with deionized water to remove the adsorbed potassium hydroxide, and stored in deionized water for at least 24 h prior to the evaluation of ionic conductivity and IEC. Any degradation in the membrane is usually observed by its structural deterioration after the process of alkaline treatment. However in the present case, no such deformation in the membrane structure was observed. Then, this membrane was clamped in the conductivity cell and its ionic conductivity was measured at different temperatures. Also the IEC of alkaline treated membrane was determined by acid-base neutralization reaction as reported in the literature.[33,34]

MEA Fabrication and Single-Cell Testing

The aforesaid membranes were evaluated in DMFC by preparing MEAs. The electrodes with the effective area of 4 cm^2 were prepared according to the procedure as follows: Commercial SIGRACET® GDL (DC-35, SGL Carbon GmbH) was used as the backing layer and the catalyst slurry was prepared in a similar manner to those reported in our earlier study.[28] Sixty weight percentage Pt-Ru (1:1 atomic ratio) supported on carbon (Vulcan-XC-72R) (Alfa Aesar, Johnson Matthey) mixed with FAA-3 ionomer (FuMA-Tech) and coated on the GDL constitutes the anode layer, while 40 wt % Pt supported on carbon (Alfa Aesar, Johnson Matthey) mixed with FAA-3 ionomer and coated on the other GDL constitutes the cathode layer. Before hot-press, the two electrodes were dipped in KOH solution (1 mol dm^{-3}) for 12 h to exchange the binder to OH^- form. MEAs were then evaluated using a conventional single cell fixture with parallel serpentine flow-field machined on graphite plates. The testing was carried out by passing 2 mol dm^{-3} aq. methanol with the flow rate of 2 mL min^{-1} on the anode side and oxygen with a flow rate of 200 mL min^{-1} on the cathode side. Measurements of cell potential as a function of current density were carried out galvanostatically using electronic load (Model-LCN4-25-24/LCN 50-24) from Bitrode Instruments (US). Also, the long-term stability of the QPPO 3 membrane in cell mode was evaluated by measuring the change in OCV as a function of time.

RESULTS AND DISCUSSION

Effect of Reaction Time in the Synthesis of CPPO

Reaction time is a very crucial parameter in the synthesis of functionalized polymers through chloromethylation. Less reaction time results in lower yield because of the incomplete functionalization; while on the other hand more reaction time results in undesirable side reactions.[35] In the present study, the reaction was performed at different time intervals (6, 8, 10, and 20 h) to investigate its effect on QPPO membrane property as shown in Table I. The degree of chloromethylation for different time intervals was calculated from the ^1H NMR spectra as represented in Figure 2 by using the equation reported in our earlier study.[28] It is evident from Table I that the DS increases as the reaction time is increased. It is found that the DS is 66% for the reaction at 20 h. But when formed as a QPPO membrane, higher swelling is observed thus reducing its stability. Similarly, the membrane fabricated from CPPO (at 10 h reaction time) also showed considerable swelling. From the above, it is concluded that the optimal reaction time for chloromethylation was 8 h with the DS of 57%. Water uptake for these membranes also quantifies the above observation as represented in Table I.

Effect of Amination in the Fabrication of Quaternized Membrane (QPPO)

Quaternization is equally an important process as chloromethylation in the preparation of AEM. Successful quaternization not only increases the ionic conductivity but can also increase the stability of the membrane. In this study, the product CPPO is aminated homogenously wherein PPO is directly converted to ionic form and is equally distributed over the polymer matrix. The amount of amine added to the polymer plays a vital role in enhancing the ionic conductivity of membrane. A series of AEMs, QPPO 1, QPPO 2, QPPO 3, and QPPO 4 were

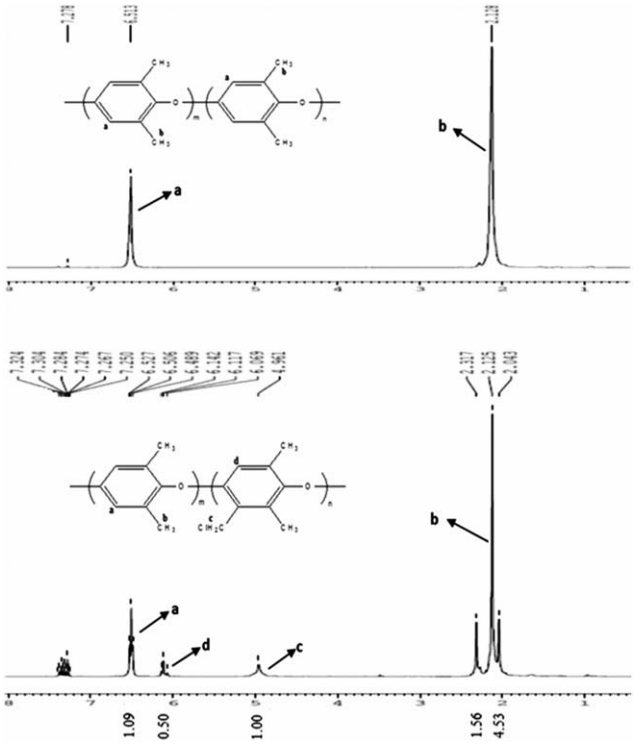

Figure 2. ^{1}H NMR spectrum of PPO and CPPO in $CDCl_3$.

fabricated with different mole ratio of amine in relation to CPPO. These membranes are equilibrated for 24 h to evaluate its ionic conductivity. As the amount of added amine increases, there is a corresponding increase in conductivity which is seen from Table II. However at higher ratio of amine, there is a decrease in ionic conductivity as well as IEC, presumably due to side reaction accelerated in the presence of excess amine. As a result of this, there will be loss of QA groups, which in turn reduces the conductivity. Among the four ratios, the QPPO 3 membrane showed better results in terms of their ionic conductivity as well as IEC. This trend is also confirmed from the DQ calculated from weight percentage of nitrogen by elemental (CHNS) analysis.[36] It is evident from Table II that the DQ increases as the ratio of amine is increased, and the maximum DQ attained was 4.31% for the membrane QPPO 3. However at higher ratio (QPPO 4) of amine, the DQ is decreased which may be due to the side reaction as described above.

Morphology for the Membranes

An important advantage of AFM in the study of surface properties is the ability to quantify both the surface morphology and surface interactions. AFM imaging was used to confirm the distributed ionic domains or clusters of QA group in the polymer. This surface microstructure can have significant impact on the properties of the membrane, particularly in the spatial arrangement of ionic sites and also to understand the hydrophilic and hydrophobic phase separation of PPO after functionalization. Figure 3 displays the AFM images for both PPO and QPPO membranes. Figure 3(a) displays the topological and three-dimensional (3D) images of the PPO membrane. As it is evident, there is no distinct phase separation where the surface is almost flat and homogenous. In the topological image of QPPO from Figure 3(b), heterogeneous morphology is observed. The dark regions correspond to the hydrophilic domains of grafted QA group, whereas the bright region is accounted for the aromatic polymeric chain.[37] As the concentration of ionic groups increase, the hydrophilic domains of QA group (dark region) predominates the bright region, which relates to increased water uptake and ionic conductivity. In the 3D-topological image of QPPO, it is seen that the ionic groups are distributed as mounds over the polymer matrix; whereas in noncontact mode imaging, the ionic clusters are clearly visible in the 3D-topological image of Figure 3(c), in which the ionic groups are spread over the entire polymer matrix which relates to facile anion transport.

Thermal Stability of Membranes

Thermal stability is an important property for the membranes to be used as polymeric electrolyte in fuel cells at elevated temperatures. Figure 4 shows the TG (thermogravimetric) curve of QPPO membranes with different mole ratio of amine. Three distinct mass losses were observed in the TG curve of all QPPO membranes. The first loss around 90 °C corresponds to the removal of absorbed water bound to the hydrophilic domains of QA group. The second mass loss observed around 160 °C indicates the detachment of QA groups from the polymer. The final weight loss observed at a temperature of 380 °C corresponds to the degradation of polymer backbone.[28] From the figure it is inferred that, as the addition of amine increases; the stability of the QA groups in the membrane also increased. Among all, the ratio of 1:4 (QPPO 1) has the lowest stability as the number of amine groups is less and the ratios 1:8 (QPPO 3) and 1:10 (QPPO 4) have increased thermal stabilities.

In order to confirm the three step degradation of QPPO membranes, the derivative thermogram (DTG) for all QPPO membranes were recorded, and are represented as a function of rate of weight change vs. temperature in Figure 4. As evident from the figure, the first peak corresponds to the loss of bound water attached to QA groups. The second peak is ascribed to the removal of QA groups from polymer whereas the third peak corresponds to the decomposition of main chain of polymer.

IEC and Ionic Conductivity

IEC of conducting membrane reflects the amount of exchangeable groups present in the membrane, and the relatively high IEC directly correlates to higher ionic conductivity. In general, increasing the fixed ion concentration leads to the increased ion-exchange capacity.[38] IECs of all QPPO membranes were evaluated by Mohr's titration method and are represented in Table II. From the table it is inferred that, as the DQ is increased, there is a corresponding increase in IEC from 0.83 (QPPO 1) to 1.38 mmol g^{-1} (QPPO 3). Among the four ratios, the membrane QPPO 3 has the highest IEC due to the increased number of QA groups attached to the polymer. However, as the ratio of amine (QPPO 4) is increased further, due to the side reaction between amine groups which could compete with the quaternization reaction, leading to decrease in the total number of QA groups established from the DQ calculated using elemental analysis.

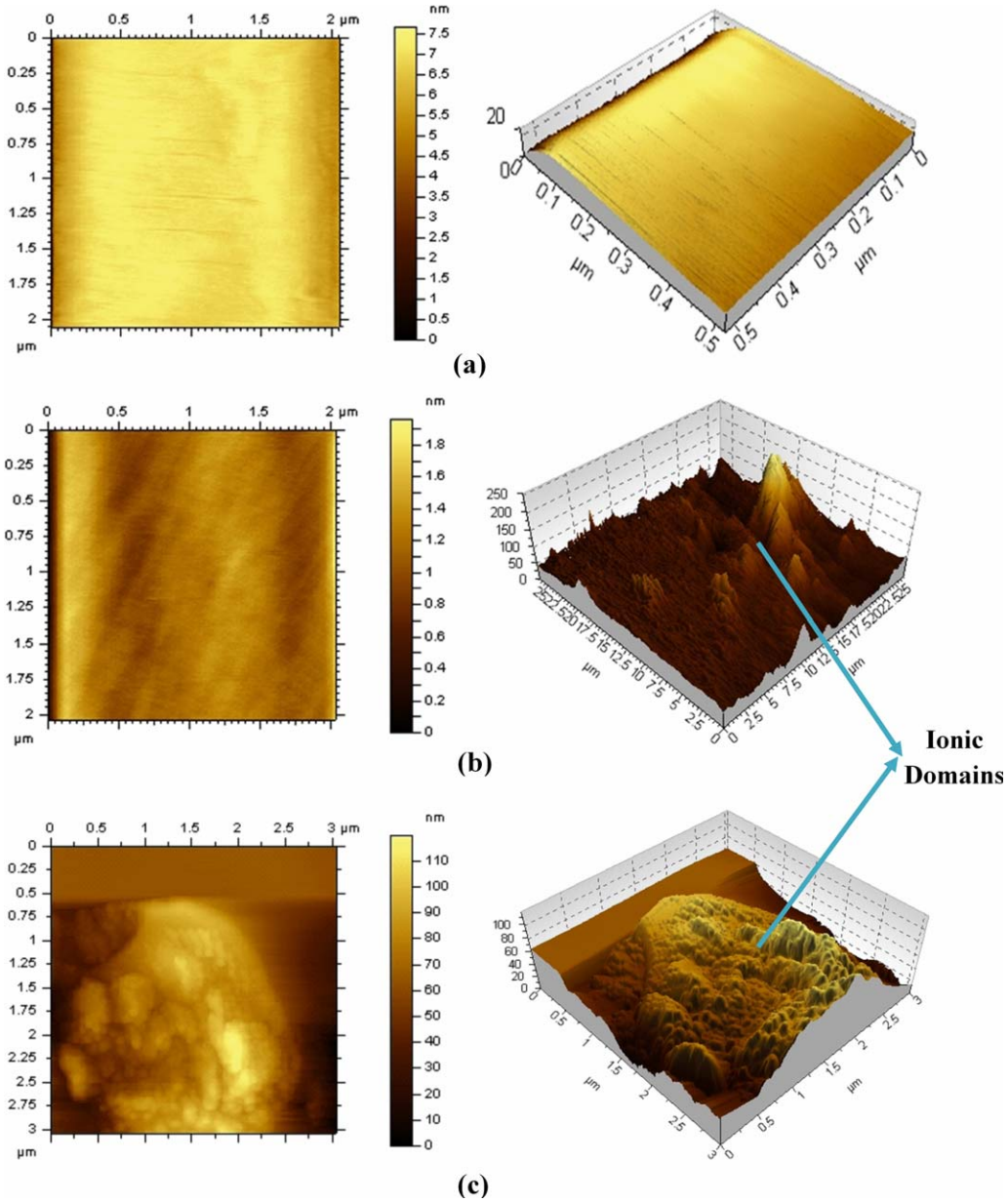

Figure 3. AFM phase and topological images of (a) PPO, (b) QPPO, and (c) noncontact mode image of QPPO membrane. [Color figure can be viewed in the online issue, which is available at wileyonlinelibrary.com.]

Ionic conductivity of an AEM is an important intrinsic parameter that plays a significant role in cell performance. It is well known that the conductivity of AEM is determined by many factors such as the degree of chloromethylation, DQ, basicity of the tethered cationic group, and micro-morphology of the membrane.[33] Further, the relationship between anion conductivity and temperature also play a potential role in ion conduction. High temperature facilitates the transport of anion, and thus the conductivity increases with temperature due to the (1) increase in inflexibility of the polymeric main chains at elevated temperatures, provides a larger free volume for enhanced ion transport and (2) faster diffusion and thermal motion of anions which improves ion conduction at higher temperatures.[39] Ionic conductivities of membranes in their chloride form were measured in order to avoid issues with the formation of carbonate ions for membranes in hydroxide form when exposed to air.

Figure 5(a) represents the ionic conductivity of QPPO membranes prepared with different mole ratio of amine as a function of temperature. As the quantity of added amine increases, there is a substantial increase in ionic conductivity. The ionic conductivity of membranes at 30 °C increased from 5.5 (QPPO 1) to 7.6 mS cm^{-1} (QPPO 3) by varying the amount of amine. The conductivity of QPPO membranes at a given temperature gradually increase in line with IEC and water uptake, with the increase in the concentration of active sites for anion transport. With the enhanced IEC from 0.83 (QPPO 1) to 1.38 (QPPO 3) mmol g^{-1}, the ionic conductivity gradually increases reaching

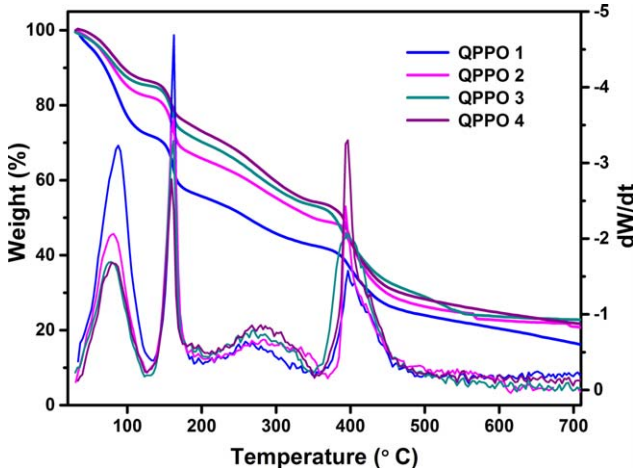

Figure 4. TG-DTG analysis for different QPPO membranes recorded at a heating rate of 5 °C min^{-1}. [Color figure can be viewed in the online issue, which is available at wileyonlinelibrary.com.]

13.9 mS cm^{-1} for the membrane QPPO 3 at 80 °C. In comparison with our earlier results,[28] the variation of reaction time on chloromethylation of PPO and the change in mole ratio of amine in QPPO has increased the ionic conductivity from 8.3 to 13.9 mS cm^{-1} with the corresponding increase in IEC from 0.7 to 1.38 mmol g^{-1}.

Activation energy, the minimum energy needed for ion transport was obtained from the slope of Arrhenius plot of ln σ vs. $1/T$ according to the equation given below:

$$\sigma = \sigma_o e^{-\left(\frac{E_a}{RT}\right)}, \quad (6)$$

where σ is the proton conductivity in S cm^{-1}, σ_o is the pre-exponential factor, R is the universal gas constant (8.314 J mol^{-1} K^{-1}), T the absolute temperature in Kelvin and E_a is the activation energy in kJ mol^{-1}. Figure 5(b) displays the Arrhenius plot for different ratio of QPPO membranes. It is observed that activation energy (E_a) decreased from 16.67 to 6.86 kJ mol^{-1} with the increase in DQ as represented in Table III. The QPPO 3 membrane has the lowest E_a of 6.86 kJ mol^{-1} among all other ratios, which is consistent with the result of its better ionic conductivity.

Methanol Permeability

In DMFC, the methanol permeability is recognized as a key factor, which not only causes the loss of fuel but also reduces performance at the cathode,[40] due to mixed potential created by reaction of methanol oxidation with the oxygen reduction reaction. Therefore, membranes with high ionic conductivity as well as low methanol permeability are strongly desired. Figure 6 shows the methanol permeability of QPPO membranes with varying DQ. Methanol permeability experiments for all the aforesaid four membranes were carried out at OCV for 5 h under identical operating conditions. As the DQ increases from 4.20 to 4.31%, there is a corresponding decrease in methanol permeability as evident from the figure. Among the four membranes, the QPPO 3 membrane has the lowest methanol permeability of 1.23×10^{-7} cm^2 s^{-1} and highest water sorption of 64% because of its higher ionic conductivity and IEC as seen from Table III. This is due to the fact that when more hydroxide ions transports from cathode to anode through the membrane; there will be a significant reduction of methanol crossover, as the hydroxide ions opposes the flow of methanol through electro-osmosis. But at higher and lower ratio of amine (QPPO 4 and QPPO 1) methanol permeability is increased probably due to their low ionic conductivity, as the total number of hydroxide ions opposing the methanol is reduced. Thus, these ratios of membranes (QPPO 1 and QPPO 4) will have higher methanol permeability as evident from the figure.

DMFC Performance Studies

Effect of Amination.. Quaternization plays a potential role in determining the performance of ADMFCs. Figure 7 shows the steady state single-cell performance curve of QPPO membranes with various mole ratio of CPPO:amine, i.e., 1:4, 1:6, 1:8, and 1:10 at 30 °C. The testing parameters are kept identical for all the four ratios. As the quantity of the amine increases, the QA groups grafted on to the polymer is increased due to the high DQ. This has a pronounced effect on the cell polarization studies as seen from the figure. It is noteworthy that a peak power density of 3.51 mW cm^{-2} with the current density of 22.5 mA

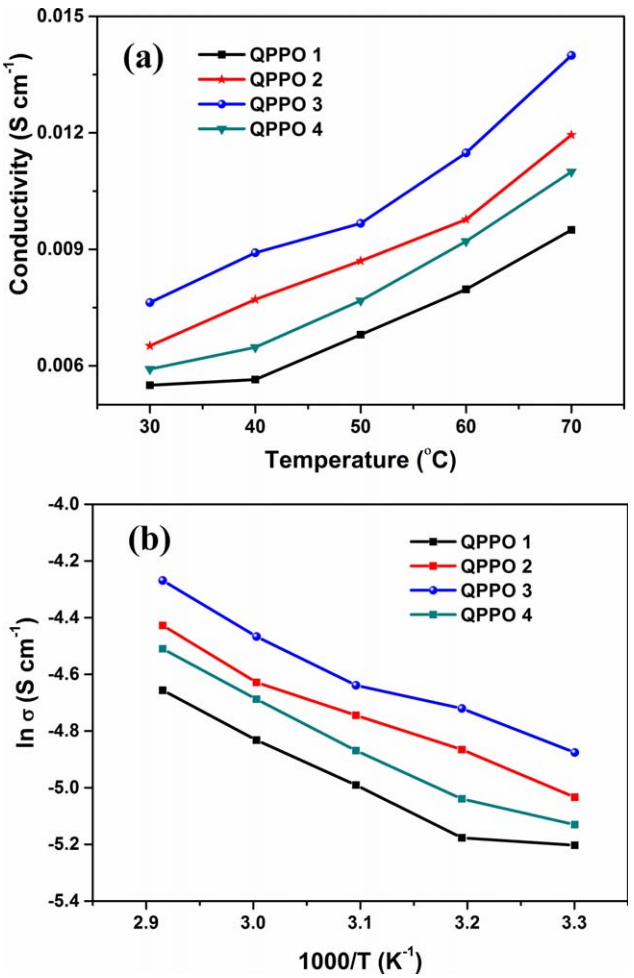

Figure 5. (a) Ionic conductivity of QPPO membranes as a function of temperature, (b) Arrhenius plot of ln conductivity vs. 1000/T for QPPO membranes. [Color figure can be viewed in the online issue, which is available at wileyonlinelibrary.com.]

Table III. Characteristic Properties of Different QPPO Membranes

Membrane type	Activation energy (kJ mol^{-1})	Water sorption at 30 °C (%)	Methanol permeability at 30 °C (10^{-7} cm^2 s^{-1})
QPPO 1	16.7	48 ± 0.2	2.43
QPPO 2	10.3	57 ± 0.1	1.52
QPPO 3	6.8	64 ± 0.1	1.23
QPPO 4	14.3	52 ± 0.2	2.32

cm^{-2} was obtained for the MEA comprising QPPO membrane with 1:8 ratio. In comparison with this, QPPO membrane with 1:6 ratio shows peak power density of 3.02 mW cm^{-2} only. However for other two ratios, namely 1:10 and 1:4, low peak power density of 1.67 and 1.20 mW cm^{-2} are attained. As expected from IEC and ionic conductivity, the ratio of 1:8 showed not only higher power density but also improved OCV when compared with other ratios. From Figure 7, it is concluded that the optimal amount of amine to be added was in the ratio of 1:8 with respect to CPPO. Janarthanan et al.[25] reported the ADMFC peak power density of 3.97 mW cm^{-2} in methanol with no hydroxide ion moiety in the fuel which is comparable with our present results.

Influence of Catalyst Loading

To understand the influence of metal content in the catalyst layer, the loading of catalyst is varied and optimized from the ADMFC performance by using QPPO 3 membrane. MEAs with different loadings such as 2, 1, and 0.5 mg cm^{-2} of Pt-Ru/C and Pt/C on both anode and cathode are evaluated and represented in Figure 8. It is to be noted that in the previous section while studying the effect of amination, the catalyst loading for all MEAs were kept constant at 2 mg cm^{-2}. As the loading in the catalyst layer decreases, the current density and power density decreased may be due to the reduced activity for oxidation and reduction. A maximum power density of 2.2 mW cm^{-2} was obtained for the MEA with 1 mg cm^{-2} catalyst loading and

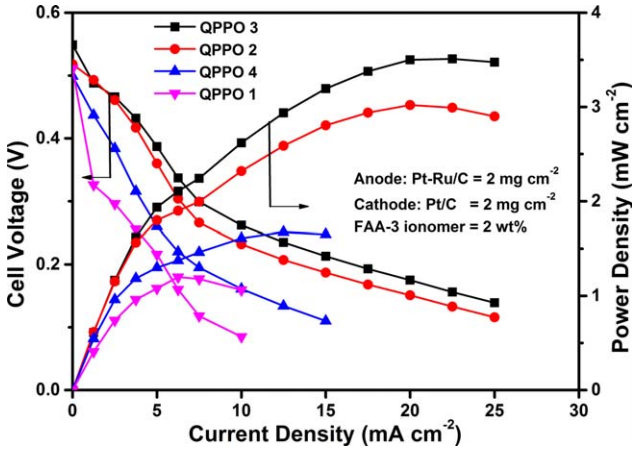

Figure 7. ADMFC performance of QPPO 1, QPPO 2, QPPO 3, and QPPO 4 membranes at 30 °C in KOH free fuel. [Color figure can be viewed in the online issue, which is available at wileyonlinelibrary.com.]

a power density of 1.4 mW cm^{-2} was obtained for MEA with 0.5 mg cm^{-2} catalyst loading on either sides. To achieve higher cell performance, the metal loading of the catalyst was increased from 2 mg to 4 mg cm^{-2}. However, during the preparation of electrodes, loading 4 mg cm^{-2} of catalyst on the gas diffusion layer was challenging. In addition to this, while immersing the electrodes in 1 mol dm^{-3} KOH solution for ion-exchange, few layers of catalyst are detached from the surface of electrodes. Hence, it is concluded that the catalyst loading of 2 mg cm^{-2} was optimal on both sides for effective ADMFC performance. To reduce the utilization of Pt-based catalysts and also to increase the cell performance, further research work is in progress for preparing non-noble metal-based catalysts.

DMFC Performance Comparison with Literature

Varcoe and Slade[41] reported an AEM from ETFE by radiation grafting with VBC monomer which showed a peak power density of 8.5 mW cm^{-2} at 80 °C in ADMFC. Even though their performance is higher than the present study, the evaluation was done by passing the feed methanol on anode and oxygen

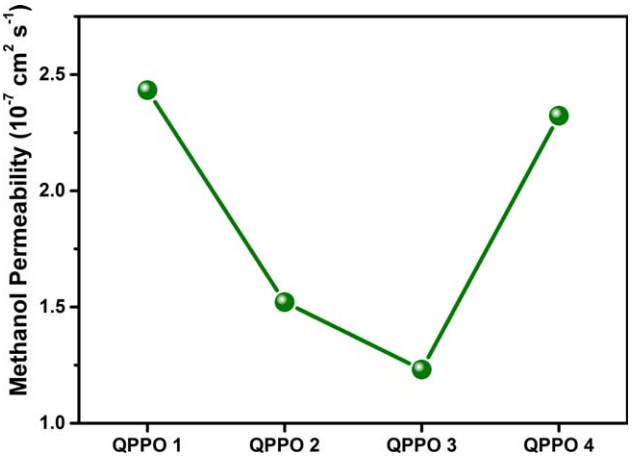

Figure 6. Methanol permeability for different QPPO membranes. [Color figure can be viewed in the online issue, which is available at wileyonlinelibrary.com.]

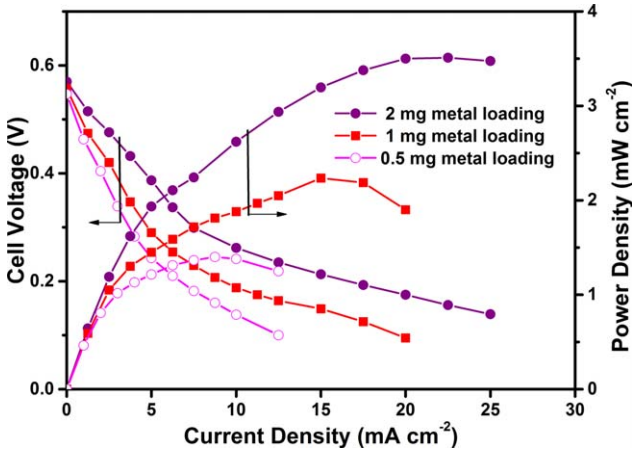

Figure 8. ADMFC polarization of QPPO 3 membrane at 30 °C with different catalyst loading in KOH free fuel. [Color figure can be viewed in the online issue, which is available at wileyonlinelibrary.com.]

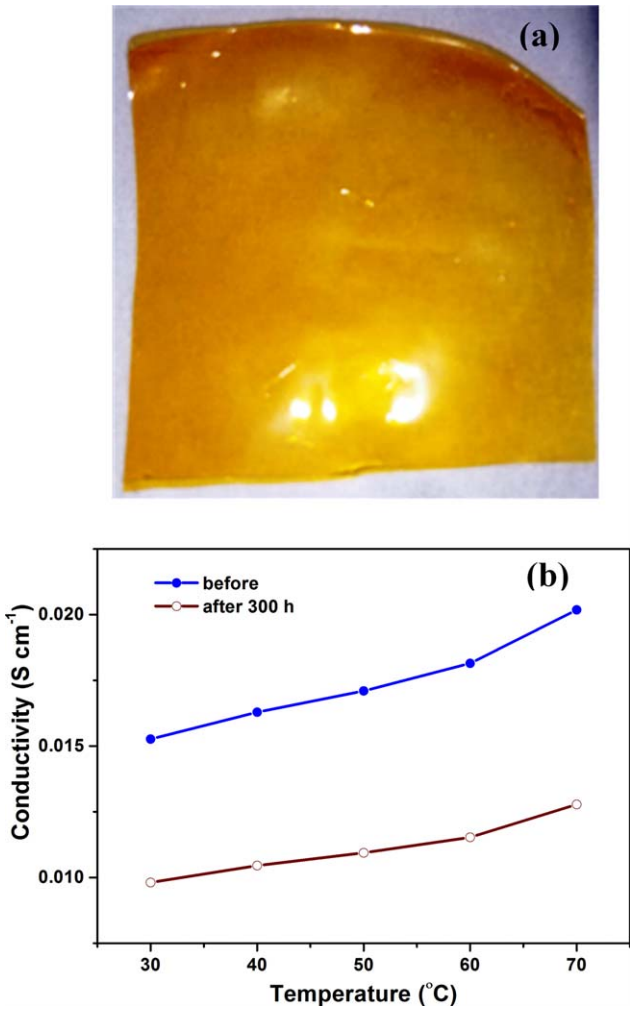

Figure 9. (a) Photograph of QPPO 3 membrane after alkaline stability, (b) stability of QPPO 3 membrane before and after alkaline treatment (with 4 mol dm^{-3} KOH at 75 °C for 300 h). [Color figure can be viewed in the online issue, which is available at wileyonlinelibrary.com.]

on cathode under 2 bar pressure condition. It is noteworthy that our present study is carried out without applying any pressurized condition where QPPO membrane showed at par results under ambient pressure. Further, Matsuoka et al.[42] reported the ADMFC performance of 6 mW cm^{-2} with commercial anion-exchange membrane at 50 °C with 4 mg cm^{-2} Pt-Ru/C loading at the anode supplied with methanol (1 mol dm^{-3}) in aqueous KOH (1 mol dm^{-3}) and 1 mg cm^{-2} Pt/C loading at the cathode supplied with oxygen. Also, Countanceau et al.[43] reported a peak power density of 18 mW cm^{-2} using methanol (2 mol dm^{-3}) with high molar KOH (4 mol dm^{-3}) solution added to the methanol feed. However, our present study avoids the above protocol to mitigate any sort of ionic conduction from aq. KOH solution.

Alkaline Stability and Durability

The stability of AEMs under alkaline conditions is another important phenomenon for its use in fuel cell because of many degradation pathways of tetra alkylammonium ions including direct nucleophilic substitution at an alpha-carbon, beta

Table IV. Alkaline Stability of QPPO Membrane at 4 mol dm^{-3} KOH for 300 h

	Ionic conductivity (OH^-) at 30 °C (mS cm^{-1})		IEC (mmol g^{-1})	
Membrane	Before	After 300 h	Before	After 300 h
QPPO 3	15	9.9	1.62	1.10

hydrogen-Hofmann elimination, or nitrogen ylide formation.[44] Generally in basic conditions, AEM degradation is possible due to the degradation of either cationic head group or the polymer backbone itself. The loss of fixed QA ions will affect the ion-exchange capacity which in turn reduces the conductivity[45] whereas the degradation of polymer backbone would cause brittleness of AEMs. The alkaline stability of optimized QPPO 3 membrane was determined by immersing the membrane sample in 4 mol dm^{-3} KOH solution at 75 °C for 300 h and the results are given in Table IV. Figure 9(a) represents the photograph of membrane after 300 h of alkaline treatment confirming no structural deformation. The ionic conductivity of membrane (in its OH^- form) was measured to observe any loss of QA groups. For comparison before alkaline treatment, the conductivity was measured separately by immersing the membrane in 2 mol dm^{-3} KOH solution at room temperature for 24 h and equilibrated in water prior to measurements. Figure 9(b) displays the ionic conductivity of QPPO 3 membrane (in OH^- form) as a function of temperature before and after alkaline stability. It is inferred from the figure that conductivity decreases but retains its major part of conductivity even after 300 h. The QPPO membrane showed a gradual decrease in QA groups of about 34% over the two week test. The decrease in conductivity is accompanied by similar decrease in IEC, confirming that the conductivity losses are due to QA degradation by S_N2 nucleophilic displacement and not by other phenomenon as reported in our previous literature.[28] The conductivity of membrane

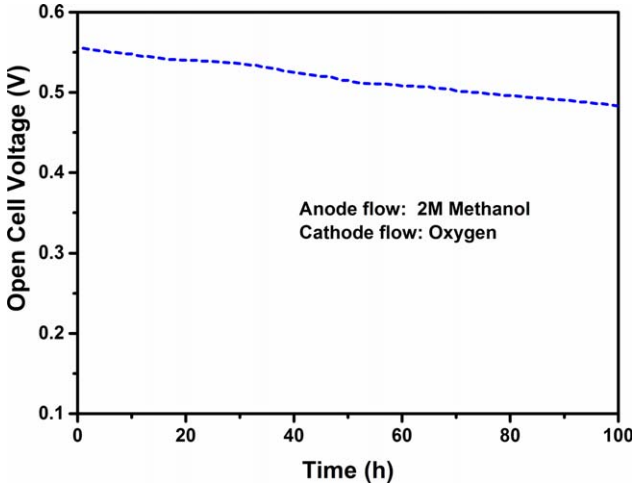

Figure 10. Long-term stability study of QPPO 3 membrane at OCV condition in KOH free media for 100 h. [Color figure can be viewed in the online issue, which is available at wileyonlinelibrary.com.]

measured before alkaline treatment was about 15 mS cm^{-1} at room temperature whereas the QPPO membrane retained its 66% conductivity of 9.9 mS cm^{-1} after 300 h.

The long-term durability of an AEM is an intrinsic parameter which plays a vital role in the stability of membrane at longer runs. The stability study for the optimized QPPO 3 membrane was carried out at OCV condition in KOH free media with 2 mol dm^{-3} methanol feed on the anode side and oxygen on the cathode side. The testing was continued for 100 h at cell temperature of 30 °C and the data are represented in Figure 10. From the figure it is seen that even though the OCV gradually varies with increase in time for 100 h, QPPO 3 membrane retain its larger part of OCV. It is inferred that the QPPO 3 membrane has higher stability with the decrease of around ~13% of OCV only even after 100 h.

CONCLUSIONS

PPO was functionalized with QA groups via chloromethylation by aryl substitution and homogenous quaternization by Menshutkin reaction. The influence of reaction time on the chloromethylation reaction was studied and optimized which play a key role in forming a stable QPPO membrane. Effect of amination on CPPO is studied by varying the amount of amine added during quaternization. A series of AEMs were prepared and evaluated for characteristic properties such as water uptake, IEC, ionic conductivity and methanol permeability. The QPPO 3 membrane exhibited a superior conductivity of 7.6 mS cm^{-1} with the lowest methanol permeability of 1.23×10^{-7} cm^2 s^{-1} at 30 °C in comparison with other ratios. An enhanced peak power density of 3.51 mW cm^{-2} with the maximum current density of 22.5 mA cm^{-2} was obtained for the MEA comprising QPPO 3 membrane in an alkaline DMFC free from KOH. Alkaline stability study concludes the fact that ionic conductivity and IEC are not much reduced for QPPO 3 membrane even after 300 h.

ACKNOWLEDGMENTS

Financial support from Council of Scientific and Industrial Research (CSIR), Govt. of India under HYDEN programme (grant number CSC0122) is gratefully acknowledged. Authors thank Director, CSIR-Central Electrochemical Research Institute for his kind support and valuable suggestions. Authors also thank Saravana Karthikeyan (CSIR-SERC) for his help in Ball-Stick model representation of the scheme.

REFERENCES

1. Aricò, A. S.; Srinivasan, S.; Antonucci, V. *Fuel Cells* **2001**, *1*, 133.
2. Dillon, R.; Srinivasan, S.; Aricò, A. S.; Antonucci, V. *J. Power Sources* **2004**, *127*, 112.
3. Neburchilov, V.; Martin, J.; Wang, H.; ; Zhang, J. *J. Power Sources* **2007**, *169*, 221.
4. Pethaiah, S. S.; Ulaganathan, M.; Viswanathan, M. R.; Chan, S. H. *RSC Adv.* **2015**, *5*, 981.
5. Wang, L.; Liu, Y.; Yang, X.; Fang, Y.; Chen, Y.; Wang, B. *J. Mater. Chem. A* **2013**, *1*, 1834.
6. Varcoe, J. R.; Slade, R. C. T. *Fuel Cells* **2005**, *5*, 187.
7. Lu, S.; Pan, J.; Huang, A.; Zhuang, L.; Lu, J. *Proc. Natl. Acad. Sci. U.S.A.* **2008**, *105*, 20611.
8. Kaspar, R. B.; Letterio, M. P.; Wittkopf, J. A.; Gong, K.; Gu, S.; Yan, Y. *J. Electrochem. Soc.* **2015**, *162*, F483.
9. Couture, G.; Alaaeddine, A.; Boschet, F.; Ameduri, B. *Prog. Polym. Sci.* **2011**, *36*, 1521.
10. Xu, T.; Liu, Z.; Li, Y.; Yang, W. *J. Membr. Sci.* **2008**, *320*, 232.
11. Gu, S.; Cai, R.; Luo, T.; Jensen, K.; Contreras, C.; Yan, Y. *ChemSusChem* **2010**, *3*, 555.
12. Wang, J.; Li, S.; Zhang, S. *Macromolecules* **2010**, *43*, 3890.
13. Page, O. M. M.; Poynton, S. D.; Murphy, S.; Ong, A. L.; Hillman, D. M.; Hancock, C. A.; Hale, M. G.; Apperley, D. C.; Varcoe, J. R. *RSC Adv.* **2013**, *3*, 579.
14. Merle, G.; Wessling, M.; Nijmeijer, K. *J. Membr. Sci.* **2011**, *377*, 1.
15. Schauer, J.; Žitka, J.; Pientka, Z.; Křivčĺk, J.; Hnát, J.; Bouzek, K. *J. Appl. Polym. Sci.* **2015**, *132*, DOI: 10.1002/app.42581.
16. Zhou, J.; Unlu, M.; Vega, J. A.; Kohl, P. A. *J. Power Sources* **2009**, *190*, 285.
17. Jasti, A.; Prakash, S.; Shahi, V. K. *J. Membr. Sci.* **2013**, *428*, 470.
18. Tanaka, M.; Fukasawa, K.; Nishino, E.; Yamaguchi, S.; Yamada, K.; Tanaka, H.; Bae, B.; Miyatake, K.; Watanabe, M. *J. Am. Chem. Soc.* **2011**, *133*, 10646.
19. Rebeck, N. T.; Li, Y.; Knauss, D. M. *J. Polym. Sci. Part B-Polym. Phys.* **2013**, *51*, 1770.
20. Stoica, D.; Ogier, L.; Akrour, L.; Alloin, F.; Fauvarque, J. F. *Electrochim. Acta* **2007**, *53*, 1596.
21. Xia, Z.; Yuan, S.; Jiang, G.; Guo, X.; Fang, J.; Liu, L.; Qiao, J.; Yin, J. *J. Membr. Sci.* **2012**, *390–391*, 152.
22. (a) Lue, S. J.; Wang, W. T.; Mahesh, K. P. O.; Yang, C. C. *J. Power Sources* **2010**, *195*, 7991. (b) Yang, C. C.; Chiu, S. J.; Chien, W. C.; Chiu, S. S.; *J. Power Sources* **2010**, *195*, 2212. (c) Yang, C. C.; Chiu, S. J.; Lee, K. T.; Chien, W. C.; Lin, C. T.; Huang, C. A.; *J. Power Sources* **2008**, *184*, 44.
23. Wan, Y.; Peppley, B.; Creber, K. A. M.; Bui, V. T. *J. Power Sources* **2010**, *195*, 3785.
24. Zhang, Y.; Fang, J.; Wu, Y.; Xu, H.; Chi, X.; Li, W.; Yang, Y.; Yan, G.; Zhuang, Y. *J. Colloid Interf. Sci.* **2012**, *381*, 59.
25. Janarthanan, R.; Pilli, S. K.; Horan, J. L.; Gamarra, D. A.; Hibbs, M. R.; Herring, A. M. *J. Electrochem. Soc.* **2014**, *161*, F944.
26. Katzfuß, A.; Gogel, V.; Jörissen, L.; Kerres, J. *J. Membr. Sci.* **2013**, *425–426*, 131.
27. Zhang, X.; Higashihara, T.; Ueda, M.; Wang, L. *Polym. Chem.* **2014**, *5*, 6121.
28. Gopi, K. H.; Peera, S. G.; Bhat, S. D.; Sridhar, P.; Pitchumani, S. *Int. J. Hydrogen Energy* **2014**, *39*, 2659.
29. Gopi, K. H.; Peera, S. G.; Bhat, S. D.; Sridhar, P.; Pitchumani, S. *Bull. Mater. Sci.* **2014**, *37*, 877.

30. Wang, C.; Shin, D. W.; Lee, S. Y.; Kang, N. R.; Robertson, G. P.; Lee, Y. M.; Guiver, M. D. *J. Mater. Chem.* **2012**, *22*, 25093.
31. Rambabu, G.; Bhat, S. D. *Electrochim. Acta* **2015**, *176*, 657.
32. Hibbs, M. R. *J. Polym. Sci. Part B-Polym. Phys.* **2013**, *51*, 1736.
33. Zhang, F.; Zhang, H.; Qu, C. *J. Mater. Chem.* **2011**, *21*, 12744.
34. Hibbs, M. R.; Hickner, M. A.; Alam, T. M.; McIntyre, S. K.; Fujimoto, C. H.; Cornelius, C. J. *Chem. Mater.* **2008**, *20*, 2566.
35. Wang, G.; Weng, Y.; Zhao, J.; Chu, D.; Xie, D.; Chen, R. *Polym. Adv. Technol.* **2010**, *21*, 554.
36. Xiong, Y.; Fang, J.; Zeng, Q. H.; Liu, Q. L. *J. Membr. Sci.* **2008**, *311*, 319.
37. Wang, Y. J.; Qiao, J.; Baker, R.; Zhang, J. *Chem. Soc. Rev.* **2013**, *42*, 5768.
38. Geise, G. M.; Cassady, H. J.; Paul, D. R.; Logan, B. E.; Hickner, M. A. *Phys. Chem. Chem. Phys.* **2014**, *16*, 21673.
39. Wang, J. L.; Wang, L. L.; Feng, R. J.; Zhang, Y. *Solid State Ionics* **2015**, *278*, 144.
40. Cruickshank, J.; Scott, K. *J. Power Sources* **1998**, *70*, 40.
41. Varcoe, J. R.; Slade, R. C. T. *Electrochem. Commun.* **2006**, *8*, 839.
42. Matsuoka, K.; Iriyama, Y.; Abe, T.; Matsuoka, M.; Ogumi, Z. *J. Power Sources* **2005**, *150*, 27.
43. Coutanceau, C.; Demarconnay, L.; Lamy, C.; Leger, J. M. *J. Power Sources* **2006**, *156*, 14.
44. Zhang, M.; Liu, J.; Wang, Y.; An, L.; Guiver, M. D.; Li, N. *J. Mater. Chem. A* **2015**, *3*, 12284.
45. Ran, J.; Wu, L.; Wei, B.; Chen, Y.; Xu, T. *Sci. Rep.* **2014**, *4*, 6486.